

Pore structure of mortars containing limestone powder and natural pozzolan assessed through mercury intrusion porosimetry and dynamic vapour sorption

Natalia Alderete^{1,*}, Yury Villagrán², Arn Mignon¹, Didier Snoeck¹, and Nele De Belie¹

¹Magnel Laboratory for Concrete Research, Department of Structural Engineering, Faculty of Engineering and Architecture, Ghent University, Tech Lane Ghent Science Park, Campus A, Technologiepark Zwijnaarde 904, B-9052 Ghent, Belgium

²LEMIT, CONICET, 52 entre 121 y 122 s/n, 1900 La Plata, Argentina

Abstract. Pore structure characterization is a key aspect when studying the durability of cementitious materials. When supplementary cementitious materials (SCMs) are used changes in pore structure are expected, and the complexity of its analysis is increased. The purpose of this paper is to describe the pore structure variation of mortars with two types of SCMs: natural pozzolan from volcanic origin (NP), and limestone powder (LP). We tested mixes with cement replacements (in weight) of 20 % and 40% by NP, and 10 % and 20% by LP. To analyse the pore structure, two widely accepted and complementary techniques were applied: dynamic water vapour sorption (DVS) and mercury intrusion porosimetry (MIP). With the DVS data, the Barret-Joyner-Halenda (BJH) model was used for pore size distribution assessment. Calculations with the Dubinin-Radushkevich (DR) model were also made for the smallest pore size range. Tests were performed at 28 and 90 days. MIP and DVS allowed evaluating the effect of the studied SCMs on different pore size ranges. Both techniques provided comprehensive information over a wide range of pore sizes. The mix with 40 % of NP had the best evolution, showing a significant volume decrease in the mesopore range.

1 Introduction

The pore structure of cementitious materials generally changes when supplementary cementitious materials (SCMs) are used. Those changes will influence directly the physical, mechanical and durability performance of the cementitious matrix. The use of non-hydraulic SCMs, such as limestone powder, results in an initial dilution effect of clinker but a facilitation of early hydration given by the generation of nucleation sites for precipitation of hydrates [1]. When using natural SCMs, such as pozzolans, there is normally an improvement in durability-related properties [2] mainly because of the delayed formation of C-S-H, which usually leads to pore refinement with time.

Although the pore structure of cementitious materials has been widely investigated [3]–[7], no unique model or method provides a complete description and characterization. Limitations include critical assumptions made for each method; it is important then to characterize the pore structure with different methods and compare the results to obtain a comprehensive description.

The mercury intrusion porosimetry (MIP) test allows to characterize the pore structure, and it has been widely applied to cementitious materials [8]–[11]. Nevertheless, its interpretation requires some theoretical simplifications, such as the same accessibility to the external surface of all the pores, and cylindrical-shaped

pores; which vary from the actual pore structures of cementitious materials. For instance, the volume of intruded mercury (ϕ_{in}) should not be associated with the total porosity but rather with the accessible porosity. Diamond [12] has described these - and other - drawbacks, but still agreed with the use of the threshold diameter (d_{th}) and ϕ_{in} as indexes of the pore structure for qualitative comparison. The d_{th} is a pore structure parameter that represents the diameter above which there is comparatively little mercury intrusion, and immediately below which starts a vast intrusion of mercury. This represents the first percolation process. The critical diameter (d_{cr}) is the most occurring diameter, and it is obtained from the derivative curve (log differential specific intruded volume - $dV/d\log(D)$ -vs. pore size). From experimental results, ϕ_{in} , d_{cr} , and d_{th} have been described to be the most representative and most useful pore parameters for modelling [13].

The dynamic vapour sorption (DVS) test provides information regarding pore structure through an experimental set-up to measure the equilibrium between the mass water content of the sample and the relative humidity (RH), at a constant temperature. Several authors have pointed out some benefits of the use of water vapour instead of other gases for sorption techniques [5], [6], [14], [15]. One of those advantages is that water molecules are relatively smaller than CO₂ or N₂ [6], which allows them to penetrate not only the small sized pores but

* Corresponding author: nataliamariel.alderete@ugent.be

also into the so-called ink-bottle pores. Moreover, it is not necessary to degas the sample prior to the measurements, hence avoiding possible microstructural damage. Nonetheless, there are some limitations in the theories of adsorption which mathematically describe the results. For instance, the monolayer of water molecules adsorbed on the pore surface is a fictional quantity and not a physical reality [16]. The Brunauer, Emmett, and Teller (BET) [17] theory implies that the surface is never completely covered until the saturated vapour pressure is reached [15]. Furthermore, calculations of the pore size distribution also have theoretical assumptions, such as the consideration of cylindrical pore shapes [16]. In spite of these limitations, isotherms may provide quantitative information, which can be used to calculate specific surface area and pore size distribution.

The purpose of this paper is to describe the pore structure of mortars with cement replacements of 20 %, and 40% by natural pozzolan of volcanic origin (NP), and 10 %, and 20 % by limestone powder (LP). MIP was performed to assess pore structure parameters, and the influence of time was evaluated on those parameters. DVS tests were performed to describe and evaluate the specific surface area and the pore size ranges.

2 Materials

Four mortar mixes were designed with a water/binder (w/b) ratio of 0.45 and a sand/binder (s/b) ratio of 3. The mixes with LP were designated as LP10, and LP20, having respectively 10 %, and 20 % of LP with respect to total binder content. The mixes with NP were designated as NP20, and NP40, having respectively 20 % and 40 % of NP with respect to total binder content. The mixing procedure was in accordance with EN 196-1 [18]. Mortar samples were cured in a conditioned room at (20 ± 2) °C and (95 ± 5) % RH, and then conditioned for testing. Ordinary Portland cement (OPC) type CEM I 42.5, normalized siliceous sand (0/2), and tap water were used in all mixes. The particle size distributions of the SCMs were characterized by laser diffractometry based on three parameters: dv_{10} , dv_{50} and dv_{90} . Each parameter is the size (in μm) below which there is 10 %, 50 % and 90 % of the volume of the sample, respectively. Values of dv_{10} , dv_{50} , and dv_{90} are 1.4, 7.1, and 28.1 for NP; and 1.3, 7.7, and 72.9 for LP.

For the MIP tests, samples were cubes with sides of approximately 15 mm, obtained from the core of cast cylinders of 75 mm height and 50 mm in diameter. To minimize microstructural damage during pre-conditioning, samples were first dried at 40 °C for 24 h and then vacuum-dried at (20 ± 2) °C for two weeks at 0.1 bar. This preconditioning technique has been validated through microstructural analyses in previous studies [15], [19]. MIP tests were performed at ages of 28 and 90 days for all mixes.

For the DVS tests, samples were obtained from the same cylinders as for the MIP tests, and manually ground and sieved between 500–1000 μm . This particle size for the sample was considered as a good compromise between test duration and practicality [15]. Carbonation

was prevented by storing samples immediately after being ground in sealed containers in the presence of soda lime until the time of testing (0.5 - 3 hours). DVS tests were performed at 28 days for all mixes. Due to the lack of refinement action of LP mixes at later ages, DVS tests at 90 days were only performed with NP mixes.

Porosity was classified, according to the guidelines provided by the International Union of Pure and Applied Chemistry (IUPAC) [20], into micropores ($<0.002 \mu\text{m}$), mesopores (0.002–0.05 μm) and macropores ($>0.05 \mu\text{m}$).

3 Methods

3.1 Mercury intrusion porosimetry

The MIP test describes the amount of mercury ingress into the sample as a function of the pressure increase. As results are based on the theoretical simplification of cylindrical pores, most pore structure parameters are defined as 'diameter'. Although this denomination has been widely accepted, it is not completely correct to describe the cementitious pore structure as a variation of diameter size.

The precise determination of d_{th} is controversial. Aligizaki [21] described it as the diameter above which there is comparatively little mercury intrusion, and immediately below which starts a vast intrusion of mercury. In order to objectively assess the value of d_{th} , several authors [13], [22], [23] have established some methods to provide comparable results. Nevertheless, this definition is still quite vague, as there is no standard procedure to determine the limit between little or vast mercury intrusion. In this paper, the calculation of d_{th} was made considering two methods:

i) *the 5% method*: this method was used in [23], where d_{th} is calculated as the point at which the intruded volume is 5% of ϕ_{in} . This offers the advantage of a conventional value and protocol, since there is no need to assume at which point sufficient mercury has penetrated into the porous system. The d_{th} obtained by using this method has been denoted as '5% pore size: $d_{5\%}$ '.

ii) *the tangent method*: this method was first adopted by Liu and Winslow [22] to determine the d_{th} . They proposed to calculate the d_{th} as the intersection of tangent lines on the cumulative distribution curve at the smallest diameter that did not exhibit significant intrusion and the largest diameter that did. Using this approach as a basis, Ma [13] fitted points at which diameters are obviously below d_{th} and above d_{th} , to determine two tangent lines. In this study, the range of the points to be fitted is determined analysing the second derivative in the differential curve. The d_{th} obtained by using this method has been denoted as 'tangent pore size: d_{tg} '.

For testing, a Pascal 140+440 mercury porosimeter with a maximum load capacity of 420 MPa was used. However, the maximum pressure was limited to 200 MPa in order to avoid cracks induced by the mercury pressure [24]. The adopted mercury surface tension and contact angle between the mercury and the solid surface were 0.482 N/m and 142°, respectively. A blank run for

differential mercury compression was made to correct the volume measurements [9]. The pore diameters related to the pressure applied were calculated with the Washburn equation [25]. The information obtained from the MIP tests was used to determine d_{lg} , $d_{5\%}$, d_{cr} , and ϕ_{in} .

3.2 Dynamic vapour sorption

The DVS test may provide valuable quantitative information regarding pore structure in a wide range of pore sizes. Although, as mentioned, there are some limitations in the theories of adsorption which mathematically describe the results. Calculations of the pore size distribution also include theoretical assumptions, such as the consideration of cylindrical pore shape.

To calculate the microstructural properties, the selection of the appropriate branch of the water isotherm is still a point for discussion. On the one hand, the sorption branch is not entirely appropriate as the menisci formation is delayed [26]. On the other hand, for the case of the desorption branch, there is a delayed evaporation or pore emptying [27]. Therefore, the results from either branch will not characterise the actual pore structure, as with the case of all techniques. For this work, the most frequently used branch - the sorption one - was considered for the calculations; all models were applied to the data from the sorption branch. This choice was also based on the shape of the isotherms, as suggested by Snoeck [26].

The Barret-Joyner-Halenda (BJH) method [28] was used for the calculation of the pore size distribution in the mesopore range (Eq. 1). This method, based on the Kelvin model, considers that capillary water and water vapour phases co-exist in cylindrical pores and calculations of the pore size distribution are made by iterative step-by-step calculations [6]. In spite of the differences between the cylindrical pore model and actual cement paste microstructure, the BJH calculation can provide useful information at least for comparative purposes [29].

$$\ln \frac{p}{p_0} = - \frac{2 \cdot \gamma \cdot \bar{V}}{r_k \cdot R \cdot T} \cdot \cos \theta \quad (1)$$

Where:

p = equilibrium vapour pressure of the liquid contained in a pore of radius r_k (%)

r_k = Kelvin radius (m)

p_0 = equilibrium pressure of the same liquid at a plane surface (%)

γ = liquid surface tension (72.8 mN·m⁻¹ at 25 °C)

\bar{V} = molar volume of liquid (mL)

θ = contact angle between the liquid and the pore wall (°)

R = universal gas constant (8.314 J K⁻¹·mol⁻¹)

T = temperature (K)

Furthermore, the Dubinin-Radushkevich (DR) equation (Eq. 2) can be used to calculate the pore size distribution in the micropore range [30]. The method is based on the assumptions of a change in potential energy between vapour and adsorbed phases.

$$\ln (W) = \ln (W_0) - \left(\frac{R \cdot T}{\beta \cdot E_0} \right)^2 \cdot \ln^2 \left(\frac{p}{p_0} \right) \quad (\text{Eq. 2})$$

Where:

W = micropore volume (mm³·g⁻¹)

W_0 = volume that has been filled at a relative pressure of p/p_0 (mm³·g⁻¹)

R = universal gas constant (8.314 J K⁻¹·mol⁻¹)

T = temperature (K)

β = affinity coefficient

E_0 = characteristic energy of adsorption for a reference vapour (J·mol⁻¹)

Furthermore, the BET theory [17] was used to calculate the specific surface area.

The device used for the water vapour sorption measurements was from Surface Measurement Systems, London, UK (Figure 1). It was set at 20 °C, and the sample weight was considered stable when the mass variation for at least five minutes was lower than 0.002 %. This limit was set as a condition to continue to the following RH level. The RH levels at which samples were subsequently equilibrated included (98–90–80–70–60–50–40–30–20–10–5–0) % RH. Since samples were taken out of the conditioned room and readily tested, they were first equilibrated to 98 % RH and then desorption-sorption cycles were performed.

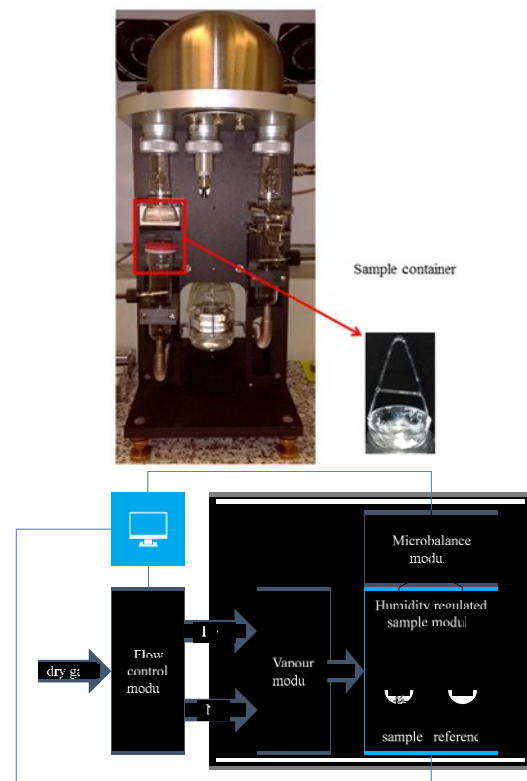


Fig. 1. Equipment used (top), schematic overview of the dynamic vapour sorption (DVS) methodology (bottom - adapted from [15]), samples container (bottom right).

4 Results and discussions

4.1 Mercury intrusion porosimetry results

As an example, Figures 2 and 3 show the intrusion curves from the MIP test of NP20 mix at 28 and 90 days, respectively. The equations obtained from the two fitting lines (dashed lines) were used for the calculation of d_{tg} . The point of intersection of those lines is the graphical representation of d_{tg} . The highest point in the curve corresponds to ϕ_{in} . The same graphical and analytical approach was used for the other mixes at 28 and 90 days. Their results are shown and discussed in section 4.3.

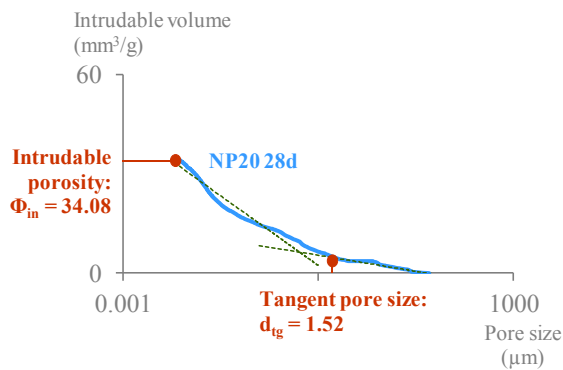


Fig. 2. Cumulative intruded volume of NP20 at 28 days with the corresponding tangent pore size (d_{tg}) and intrudable porosity (ϕ_{in}).

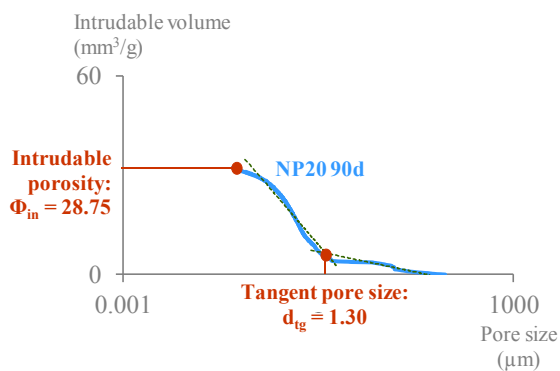


Fig. 3. Cumulative intruded volume of NP20 at 90 days with the corresponding tangent pore size (d_{tg}) and intrudable porosity (ϕ_{in}).

4.2 Dynamic vapour sorption results

Desorption-sorption isotherms of NP20 are shown in Figures 4 and 5 at 28 and 90 days, respectively. Curves of desorption have square markers and sorption curves have circle markers. The maximum moisture sorption at 98 % RH is marked. The decrease in these values indicates a decrease in the moisture uptake of the sample. For the NP20 mix this value was reduced with 21.9 % from 28 to 90 days. For the NP40 mix this value was reduced with 33.1 % from 28 to 90 days.

From the information obtained from the isotherms, the volume of micropores, mesopores and the specific surface area were calculated. Results of all mixes are shown and discussed in section 4.3.

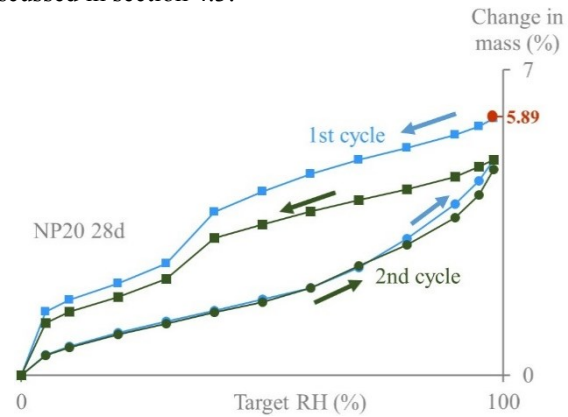


Fig. 4. Desorption and sorption isotherm curves of NP20 at 28 days.

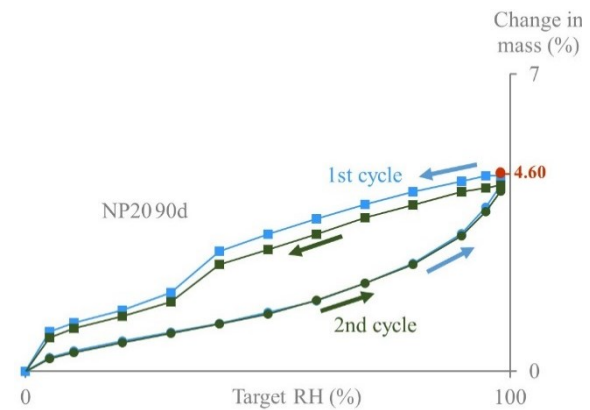


Fig. 5. Desorption and sorption isotherm curves of NP20 at 90 days.

4.3 Comparisons and discussions

Figure 6 shows the values of d_{tg} (triangle marker), $d_{5\%}$ (square marker), and d_{cr} (circle marker) obtained from the MIP results for all mixes at 28 and 90 days. Because values of d_{cr} are relatively small, the left axis shows the values of d_{tg} and $d_{5\%}$, and the right axis the values of d_{cr} .

Although the 5% method offers a conventional and simple calculation for the threshold diameter, $d_{5\%}$ does not seem to be an accurate pore size descriptor. According to this parameter, the size of the threshold diameter seems to be smaller for LP mixes than for NP mixes. It is possible that the dilution effect of LP is compensated by the enhancement of nucleation sites at 28 days. However, $d_{5\%}$ even increased after 90 days for LP20 and NP40 mixes.

For the case of the d_{tg} , values decreased with increasing LP and NP content. Values of d_{tg} of LP20 and NP40 mixes are lower than d_{tg} values from LP10 and NP20 mixes, respectively, both at 28 and 90 days. Still, the reduction at 90 days of the d_{tg} values for NP mixes was higher than for LP mixes, due to the pozzolanic action of NP. Particularly NP40 had the smallest d_{tg} value at 90 days.

While d_{cr} values seem to vary significantly, the size changes are small. All mixes have a d_{cr} value between $0.01 \mu\text{m}$ and $0.05 \mu\text{m}$, so all still are in the mesopore range, which is nearly the limit of the pore size measurement that MIP can detect.

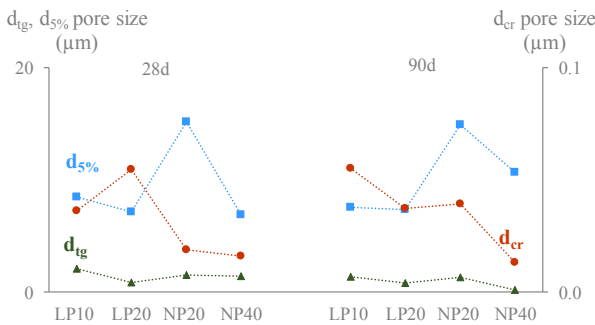


Fig. 6. Pore size parameters obtained from MIP data for all mixes at 28 and 90 days. Values of d_{tg} (triangle marker), and $d_{5\%}$ (square marker) are represented on the left vertical axis, and values of d_{cr} (circle markers) on the right vertical axis.

All mixes exhibited a Type IV isotherm shape [31], and a marked hysteresis typical of cementitious materials. The desorption branch generally shows an abrupt decrease after 40 % RH in every case, whereas in the case of the sorption curve, there is a steep rise above 60 % RH, showing that a cementitious matrix is mainly composed of mesopores. This behaviour can be explained by constriction or choke point effects of the microstructure [11], on the basis of a similar hypothesis to that used for MIP data. In this sense, Snoeck et al.[15] suggested that mainly ink bottle pores may be responsible for this steep decrease. They explained that if the diameter of the pore entrance or choke point is smaller than a certain critical width, the mechanism of desorption from the pore body involves the spontaneous nucleation and growth of vapour bubbles in the metastable condensed fluid. In this case, the body empties while the pore neck remains filled. In the case of the sorption curve, the steep rise above 60 % RH shows the menisci formation in the pores. This leads to the marked hysteresis noticed in all the curves. The different path followed by the desorption and the sorption curve has been described in many cases for porous materials [6], [26], [32]–[34]. The network theory explains this hysteretic behaviour considering the existence of controlling pore size entries that govern the dynamics of water ingress [26]. In that sense, the net pore volume also has less influence than the pore connectivity and the presence of restrictive pore sizes on the accessibility into the matrix. The different paths inside the microstructure define to what extent the water inside the pores vaporizes or condensates according to their connectivity.

For all the mixes tested, isotherms show a variation between the initial water content and the water content at the end of the first cycle (water content at the end of the first sorption branch). The high initial moisture content gained by being kept in a conditioned room at $\text{RH} > 95 \%$ during curing was not reached again afterwards. Furthermore, from the second desorption curves, the whole branch seems to have lower values than the initial

one, especially above 50 % RH. Similar results were found in cement pastes with slag and pozzolans [29]. The instability of the pore structure during the first desorption can be the cause of this difference, as drying below 40 % RH causes irreversible collapse of low density C-S-H [35], [36] and thus changes the C-S-H into a stiffer, stronger and denser one. The pore structure is considered more stable after this first desorption. To avoid the risk of damaging the pore structure, De Belie et al. [29] stopped the desorption at 10 % RH, but the difference at medium to high RH between first and second desorption curves was still noticed. Furthermore, at the end of the second sorption when the RH was further decreased to 0 % in the second desorption curve the difference was not larger. Then, they concluded that the difference between first and subsequent desorption curves was not caused by a change in the pore structure.

The pore structure description obtained from the DVS tests is shown in Figure 7. For the case of LP mixes, the volume of mesopores is lower in the LP20 mix than in the LP10 mix, in correspondence with the decrease in the d_{tg} value. Still, the mix with 20 % of NP has less volume of mesopores than the mix with same amount of LP, even at 28 days. The volume of micropores is also higher for NP20 than for LP20. These results indicate a more ‘refined’ pore structure of the mix with NP. Results at 90 days of both NP20 and NP40 mixes show the pore refinement action, especially seen for NP40 in the mesopore range. This is in agreement with the smallest d_{tg} found for NP40 from MIP results.

Remarkably, values from the specific surface calculated with the BET theory follow the same trend as the amount of micropores calculated with the DR equation. This shows the dominant influence of the micropore range size on the specific surface area.

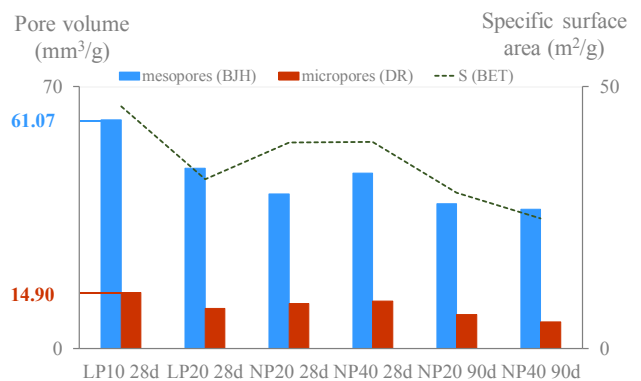


Fig. 7. Pore structure description obtained from DVS data. Volumes of mesopores (BJH) and micropores (DR) are represented on the left vertical axis. Specific surface areas (BET) are represented on the right vertical axis.

For comparison purposes, both micropore and macropore pore volumes were added to obtain a (virtual) total pore volume from the DVS data. Similarly, the intrudable porosity by mercury can be considered as a virtual total pore volume. The comparison is made to contrast the porosity accessible to water molecules (DVS results) and the porosity accessible to mercury (MIP results) (Figure 8). Values from DVS data are higher for all mixes, since this technique covers a wider pore size

range than the MIP technique. Water molecules can penetrate the smallest pores of the micropore range, while this is not possible for the case for MIP. This difference has also been found by [33] and accounted for the differing abilities of these methods for sampling different pore sizes. Despite their different measurement range, there is a good agreement on the global tendency.

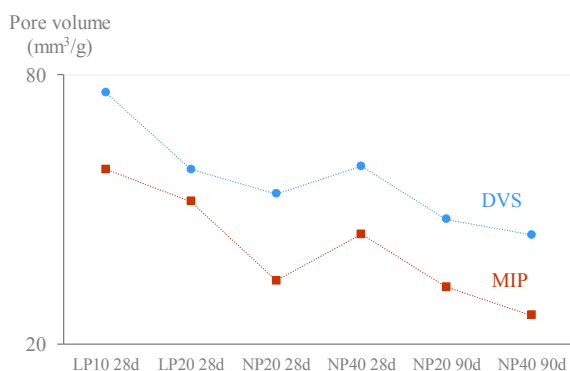


Fig. 8. Comparison between the porosity accessible to water molecules (DVS results) and the porosity accessible to mercury (MIP results).

5 Conclusions

Both DVS and MIP tests were able to characterize the pore size distribution of mortar mixes with partial replacement of cement by natural pozzolan or limestone powder.

When comparing pore size distribution over time, the NP40 mix had the best evolution, showing a significant volume decrease especially in the mesopore range. This was detected by the decrease in the d_{lg} and ϕ_m values, from the MIP results. The results from DVS test also showed that the NP40 mix has the largest reduction of pore volume in the mesopore and micropore ranges.

While MIP and DVS techniques do not cover the same range of pore sizes, both provide valuable information about the ‘computable’ pore volume that each method can measure. Differences in the values obtained with DVS and MIP are attributed to the actual differences in the measurements that both methods perform and in range of the pore sizes they describe.

The data provided by both methods can be considered complementary to each other. The simultaneous use of both techniques gives comprehensive information over a wide range of pore sizes.

The contribution of Natalia Alderete and Yury Villagrán was partially funded by PICT 0126-2013, from ANPCyT (MINCyT). As a Postdoctoral Research Fellow of the Research Foundation-Flanders (FWO-Vlaanderen), D. Snoeck would like to thank the foundation for the financial support (12J3617N).

References

[1] Y. A. Villagrán Zaccardi, Á. A. Di Maio, and R. Romagnoli, *MRS Proc.*, vol. 1488, 2012.
[2] M. Najimi, J. Sobhani, B. Ahmadi, and M. Shekarchi, *Constr. Build. Mater.*, vol. **35**, pp. 1023–

1033, 2012.
[3] S. Bahador and H. C. Jong, *32nd Conf. Our World Concr. Struct.*, pp. 10003201801–10003201811, 2007.
[4] X. Chen, S. Wu, and J. Zhou, *Appl. Clay Sci.*, vol. **101**, pp. 159–167, 2014.
[5] M. Wua, B. Johannesson, and M. Geiker, *Constr. Build. Mater.*, vol. **66**, pp. 621–633, 2014.
[6] V. Baroghel-Bouny, *Cem. Concr. Res.*, vol. **37**, no. 3, pp. 414–437, 2007.
[7] V. Baroghel-Bouny, M. Thiéry, and X. Wang, *Cem. Concr. Res.*, vol. **41**, no. 8, pp. 828–841, 2011.
[8] D. N. Winslow, M. D. Cohen, D. P. Bentz, K. A. Snyder, and E. J. Garboczi, *Cem. Concr. Res.*, vol. **24**, no. 1, pp. 25–37, 1994.
[9] R. A. Cook and K. C. Hover, *Cem. Concr. Res.*, vol. **29**, pp. 933–943, 1999.
[10] C. Leech, D. Lockington, and R. D. Hooton, *ACI Struct. J.*, vol. **103**, no. 2, pp. 291–295, 2006.
[11] D. K. Panesar and J. Francis, *Constr. Build. Mater.*, vol. **52**, pp. 52–58, 2014.
[12] S. Diamond, *Cem. Concr. Res.*, vol. **30**, no. 10, pp. 1517–1525, 2000.
[13] H. Ma, *J. Porous Mater.*, vol. **21**, no. 2, pp. 207–215, 2014.
[14] Q. Zeng, D. Zhang, H. Sun, and K. Li, *Mater. Charact.*, vol. **95**, pp. 72–84, 2014.
[15] D. Snoeck, L.F. Velasco, A. Mignon, S. Van Vlierberghe, P. Dubruel, P. Lodewyckx, N. De Belie, *Cem. Concr. Res.*, vol. **64**, pp. 54–62, 2014.
[16] L. F. Velasco, D. Snoeck, A. Mignon, L. Misseeuw, C.O. Ania, S. Van Vlierberghe, P. Dubruel, N. De Belie, P. Lodewyckx, *Carbon N. Y.*, vol. **106**, pp. 284–288, 2016.
[17] Brunauer, S. Macko, P. H. E. Emmett, Teller, and Edward, *J. Am. Chem. Soc.*, vol. 60, pp. 309–319, 1938.
[18] NBN EN 196-1, ‘Methods of testing cement - Part 1 : Determination of strength’, *Bur. voor Norm.*, 2016.
[19] J. Zhang and G. W. Scherer, *Cem. Concr. Res.*, vol. **41**, no. 10, pp. 1024–1036, 2011.
[20] K. S. W. Sing, D.H. Everett, R.A.W. Haul, L. Moscou, R.A. Pierotti, J. Rouquerol, T. Siemieniewska, *Pure Appl. Chem.*, vol. 57, no. 4, pp. 603–619, 1985.
[21] K. K. Aligizaki, *Pore structure of cement-based materials: testing, interpretation and requirements*. London, 2005.
[22] Z. Liu and D. Winslow, *Cem. Concr. Res.*, vol. **25**, no. 4, pp. 769–778, 1995.
[23] P. Pipilikaki and M. Beazi-Katsioti, *Constr. Build. Mater.*, vol. **23**, no. 5, pp. 1966–1970, 2009.
[24] J. J. Beaudoin and J. Marchand, ‘Pore Structure’, *Handb. Anal. Tech. Concr. Sci. Technol.*, pp. 528–628, 2001.

- [25] E. W. Washburn, *J. Phys. Rev.*, no. **17**, pp. 273–283, 1921.
- [26] D. Snoeck, ‘Self-Healing and Microstructure of Cementitious Materials with Microfibres and Superabsorbent Polymers’, Ghent University, 2015.
- [27] A. Korpa and R. Trettin, *Cem. Concr. Res.*, no. **36**, pp. 634–649, 2006.
- [28] E. Barret, L. Joyner, and P. Halenda, *J. Am. Chem. Soc.*, vol. **73**, pp. 373–380, 1951.
- [29] N. De Belie, J. Kratky, and S. Van Vlierberghe, *Cem. Concr. Res.*, vol. **40**, no. 12, pp. 1723–1733, 2010.
- [30] M. M. Dubinin, *Prog. Surf. Membr. Sci.*, vol. **9**, pp. 1–70, 1975.
- [31] S. Brunauer, L. S. Deming, W. E. Deming, and E. Teller, *J. Am. Chem. Soc.*, vol. **62**, no. 7, pp. 1723–1732, Jul. 1940.
- [32] D. Dollimore, P. Spooner, and A. Turner, *Surf. Technol.*, vol. **4**, pp. 121–160, 1976.
- [33] P. A. Monson, *Microporous Mesoporous Mater.*, vol. **160**, pp. 47–66, 2012.
- [34] A. Kumar, S. Ketel, K. Vance, T. Oey, N. Neithalath, and G. Sant, *Transp. Porous Media*, vol. **103**, no. 1, pp. 69–98, 2014.
- [35] H. M. Jennings, *Cem. Concr. Res.*, vol. **30**, no. 1, pp. 101–116, Jan. 2000.
- [36] J. J. Thomas and H. M. Jennings, *Cem. Concr. Res.*, vol. **36**, no. 1, pp. 30–38, 2006.